Embedding carbon dots and gold nanoclusters in metal-organic frameworks for ratiometric fluorescence detection of Cu²⁺

Qingqing Tan[1] · Ruirui Zhang[2] · Guoyan Zhang[1] · Xiaoya Liu[1] · Fengli Qu[1] · Limin Lu[3]

Abstract

Herein, a dual-emission metal-organic framework based ratiometric fluorescence nanoprobe was reported for detecting copper(II) ions. In particular, carbon dots (CDs) and gold nanoclusters (AuNCs) were embedded into ZIF-8 (one of the classical metal-organic frameworks) to form CDs/AuNCs@ZIF-8 nanocomposites, which exhibited dual-emission peaks at UV excitation. In the presence of Cu^{2+}, the fluorescence attributed to AuNCs can be rapidly quenched, while the fluorescence of CDs serves as reference with undetectable changes. Therefore, the CDs/AuNCs@ZIF-8 nanocomposites were utilized as a ratiometric fluorescence nanoprobe for sensitive and selective detection of Cu^{2+}. A good linear relationship between the ratiometric fluorescence signal of CDs/AuNCs@ZIF-8 and Cu^{2+} concentration was obtained in the range of 10^{-3}–10^3 μM, and the detection limit was as low as 0.3324 nM. The current ratiometric fluorescence nanoprobe showed promising prospects in cost-effective and rapid determination of Cu^{2+} ions with good sensitivity and selectivity. Furthermore, this nanoprobe has been successfully applied for the quantitative detection of Cu^{2+} in serum samples, indicating its value of practical application.

Keywords Metal-organic frameworks · Ratiometric fluorescence nanoprobe · Copper · Carbon dots · Gold nanoclusters

Introduction

Copper is one of important elements for human health, which plays pivotal functions in multiple physiological processes dependent on the copper homeostasis in the human body

Qingqing Tan and Ruirui Zhang contributed equally to this work.

Electronic supplementary material The online version of this article (https://doi.org/10.1007/s00216-019-02353-5) contains supplementary material, which is available to authorized users.

✉ Fengli Qu
  fengliquhn@hotmail.com

✉ Limin Lu
  lulimin816@hotmail.com

1   College of Chemistry and Chemical Engineering, Qufu Normal University, Qufu 273165, Shandong, China

2   College of Chemistry, Chemical Engineering and Materials Science, Key Laboratory of Molecular and Nano Probes, Ministry of Education, Shandong Provincial Key Laboratory of Clean Production of Fine Chemicals, Shandong Normal University, Jinan 250014, Shandong, China

3   Institute of Functional Materials and Agricultural Applied Chemistry, College of Science, Jiangxi Agricultural University, Nanchang 330045, Jiangxi, China

[1]. Excessive copper ions in the body would disturb the cellular homeostasis that causes Alzheimer's, Wilson, and Menkes diseases [2–4]. Consequently, the accurate detection of copper is of great importance in disease diagnosis. Up to now, a number of methods have been developed for the detection of Cu^{2+}, such as colorimetric [5, 6], fluorescence [7, 8], electrochemistry [9], chemiluminescence [10], and Raman spectroscopy [11]. Among them, the fluorescence assay may be a good alternative due to the advantages of high precision and repeatability. So far, some fluorescent probes have been used for detecting Cu^{2+}, but the most among that have single-wavelength emission which is the only detection signal [12–15]. In this case, factors such as probe concentration, environmental conditions, and instrumental efficiency would cause negative effects for the output of detection signal [16]. Ratiometric fluorescent probes are of particular interest since they could provide intrinsic reference to eliminate most or all interferences by self-calibration of two emission bands [17, 18].

Recently, various ratiometric fluorescent probes have been designed and fabricated [19–23]. Among them, nanohybrids have attracted more attentions compared to organic dyes, owing to their better stability with respect to photobleaching, higher fluorescence quantum yield, and easier preparation

[24, 25]. Generally, these nanohybrids were assembled by combining two different fluorescent nanoparticles, in which one fluorophore as reference and another as a signal report unit. In present, the nanohybrids based on metal-organic framework materials (MOFs) exhibit attractive properties, which have outstanding benefits that derive from the incorporated foreign nanomaterials [26–29]. Several reports have demonstrated introducing guest nanomaterials with versatile shapes and functions into ZIF-8 is an important way to synthesize ideal luminescence-functionalized MOFs for chemical sensing [30–33]. Moreover, the accumulation effect of MOFs can greatly amplify the signal of incorporated nanomaterials [27]. For example, Chen et al. reported encapsulating fluorescent carbon quantum dots (CDs) into ZIF-8 to form CDs@ZIF-8 for ultrasensitive chemical sensing of Cu^{2+} in environmental water samples [34]. However, the fluorescence probes with single "turn-off" mode usually generate false-positive results, which restrict their practical applications.

Herein, we reported a dual-emission fluorescent nanoprobe CDs/AuNCs@ZIF-8 for the detection of Cu^{2+}. The sensitivity and accuracy for detecting Cu^{2+} were greatly improved by the self-calibration ability of dual-emission fluorescent nanoprobe. The CDs/AuNCs@ZIF-8 nanocomposites with dual-emission peaks were constructed by embedding carbon dots (CDs) and gold nanoclusters (AuNCs) into ZIF-8. Interestingly, in the presence of Cu^{2+}, the fluorescence which belonged to AuNCs could be responded rapidly by quenching, while the fluorescence of CDs served as reference with negligible change. Furthermore, the proposed ratiometric fluorescence nanoprobe could rapidly detect Cu^{2+} in cost-effective and showed good selectivity and anti-interference ability.

Experimental section

Reagents and apparatus

Glutathione (GSH), 2-methylimidazole, cysteine (Cys), glycine (Gly), phenylalanine (Phe), tyrosine (Tyr), glutamate (Glu), and aspartic acid (Asp) were purchased from Aladdin Chemical (Shanghai, China). Tripolycyanamide, sodium citrate, zinc nitrate hexahydrate ($Zn(NO_3)_2 \cdot 6H_2O$), chloroauric acid ($HAuCl_4$), sodium dihydrogen phosphate dihydrate ($NaH_2PO_4 \cdot 2H_2O$), sodium monohydrogen heptahydrate phosphate ($Na_2HPO_4 \cdot 7H_2O$), copper nitrate ($Cu(NO_3)_2$), zinc chloride ($ZnCl_2$), sodium chloride (NaCl), magnesium chloride hexahydrate ($MgCl_2 \cdot 6H_2O$), iron sulfate hydrate ($FeSO_4 \cdot 7H_2O$), lead nitrate ($Pb(NO_3)_2$), and alchlor ($AlCl_3$) were bought from Sinopharm Chemical Reagent Co., Ltd. (Shanghai, China). All the reagents were of analytical grade and used without further purification. All the solutions were prepared using phosphate buffer solution (PBS).

Transmission electron microscopy (TEM) were carried out with a JEM-2100 PLUS microscope (Japan). Fourier transform infrared spectrometry (FTIR) spectrum was recorded with a Beifen-Ruili WQF-520A FTIR spectrometer (China). Ultraviolet-visible (UV-vis) absorption spectra were recorded using a Varian Cary-300 bio UV/vis spectrophotometer (USA). The fluorescence lifetime was studied by a Fluorolog-3-21 spectrometer (USA). All fluorescence measurements were carried out with a Hitachi F-7000 spectrometer (Japan). The instrument parameters were set as follows: $\lambda_{ex} = 365$ nm (slit = 10 nm), $\lambda_{em1} = 462$ nm (slit = 10 nm), $\lambda_{em2} = 574$ nm (slit = 10 nm), PMT detector voltage = 400 V.

Synthesis of CDs

The CDs was prepared via the method documented in previous report with minor modification [35]. Specifically, 0.24 g of tripolycyanamide, 0.58 g of sodium citrate, and 25 mL of distilled water were mixed and sonicated for 5 min to form homogeneous mixture solution. The above solution was then transferred to a 50 mL Teflon-lined autoclave. After hydrothermal reaction proceeded at 180 °C for 12 h, the mixture was filtered with a cylinder membrane filter (0.22 μm) to remove the large particles, and dialyzed against ultrapure water through a 500 D of dialysis membrane for 48 h. The as-prepared CDs were stored at 4 °C for further use.

Synthesis of luminescent AuNCs

The luminescent AuNCs were synthesized according to the literature [36]. In brief, $HAuCl_4$ (20 mM, 0.50 mL) and GSH (100 mM, 0.15 mL) were mixed with 4.35 mL ultrapure water at 25 °C. The reaction mixture was gently stirring (500 rpm) for 24 h at 70 °C. The resultant orange-emitting AuNCs solution was stored at 4 °C for further use.

Synthesis of CDs/AuNCs@ZIF-8

The preparation of CDs/AuNCs@ZIF-8 nanocomposites was carried out by a one-pot method with minor modification [31, 37]. Typically, a certain volume of CDs and AuNCs mixture was added into $Zn(NO_3)_2$ aqueous solution, after ultrasonic dispersion for 30 min, rapidly injecting the mixture into 2-methylimidazole aqueous solution with molar ratio of Zn^{2+}:2-methylimidazole: $H_2O = 1:70:1238$ under vigorous stirring. After a 10-min reaction, the resultant precipitate was centrifuged, washed, and vacuum-dried at 50 °C to get the powder. The CDs/AuNCs@ZIF-8 nanoprobe was obtained by dissolving the powder with buffer solution. The fluorescence intensity of CDs/AuNCs@ZIF-8 could be regulated by varying the volume of AuNCs and CDs solution.

General procedure for detecting Cu²⁺

In a typical process, the CDs/AuNCs@ZIF-8 nanocomposites solutions and Cu²⁺ solutions were prepared with buffer solution (PBS = 7.4, 10 mM). Nine hundred microliters of CDs/AuNCs@ZIF-8 nanocomposites solution and 100 μL of Cu²⁺ solutions with different concentrations (1 nM–1 mM) were incubated for 10 min at room temperature; then, the fluorescence intensity of the mixture at 462 nm and 574 nm was measured at excitation wavelength of 365 nm.

Results and discussion

Possible mechanism of Cu²⁺ determination

The possible principle of CDs/AuNCs@ZIF-8 nanoprobe for detecting Cu²⁺ is illustrated in Scheme 1. The CDs/AuNCs@ZIF-8 nanocomposites were successfully synthesized by mixing CDs and AuNCs in the presence of Zn(NO₃)₂ and 2-methylimidazole (the precursors of ZIF-8). The CDs/AuNCs@ZIF-8 nanocomposites exhibited dual-emission peaks at 365 nm excitation. The fluorescence peak at 462 nm was attributed to the transition from LUMO to HOMO orbitals of the CDs [38], and the remarkable luminescence of AuNCs (574 nm) was attributed to the electronic interband transitions in occupied "sp" and "d" bands (LUMO-HOMO) [39]. After the addition of Cu²⁺, the 574 nm emission peak was quenched drastically, while the fluorescence at 462 nm remained almost unchanged. The phenomenon could be explained by that Cu²⁺ could coordinate with -COOH of GSH on the surface of AuNCs, leading to the quench of AuNCs fluorescence.

To explore whether the quenching process was static or dynamic, fluorescence lifetimes of AuNCs in the absence or presence of Cu²⁺ were investigated (Fig. 1a). As shown in Table S1 (see Electronic Supplementary Material, ESM), fluorescence lifetimes of AuNCs and AuNCs + Cu²⁺ were 581.18 ns and 56.69 ns, respectively. The fluorescence lifetime of AuNCs was obviously shorten by adding Cu²⁺, revealing that Cu²⁺-triggered quenching process could be attributed

to dynamic quenching [40]. This result was consistent with the fluorescence spectra of AuNCs + Cu²⁺ (Fig. 1b). Besides, the fluorescence spectra of CDs in the absence or presence of Cu²⁺ were also explored (Fig. 1c), the difference of the fluorescence intensity of CDs with and without Cu²⁺ is negligible. That could be for the interaction between Cu²⁺ and CDs was too weak to affect the fluorescence of CDs. The above mechanism was confirmed again by fluorescence spectra of CDs/AuNCs@ZIF-8 + Cu²⁺ (Fig. 1d).

Characterization of CDs/AuNCs@ZIF-8

The morphology and size of synthesized CDs/AuNCs@ZIF-8 nanocomposites were observed by the transmission electron microscopy (TEM). As illustrated in Fig. 2a, the prepared CDs with an average size of 4–6 nm were uniform and monodispersed with a quasi-spherical shape. The high-resolution TEM (HRTEM) image of CDs (the inset in Fig. 2a) showed the spacing of the adjacent lattice planes for random nanoparticle were 0.25 nm, which agrees well with the (100) diffraction plane of graphite. That indicated the prepared CDs possess a graphite-like structure. Figure. 2b revealed the typical TEM image of AuNCs; the size of AuNCs was about 2 nm. The inset in Fig. 2b demonstrated the HRTEM image of AuNCs, the spacing of the adjacent lattice planes for AuNCs were 0.235 nm, which were in accord with the previous reports [23]. Figure 2c and d manifested the pure ZIF-8 and CDs/AuNCs@ZIF-8 nanocomposites, respectively. The CDs/AuNCs@ZIF-8 exhibited a hexagonal shape with the size of approximately 175 nm (see Fig. S1 in the ESM). The difference of between CDs/AuNCs@ZIF-8 nanocomposites and pure ZIF-8 was negligible, which was well coincide with the previous studies [27, 31, 32]. The consistency in size and shape between the CDs/AuNCs@ZIF-8 and pure ZIF-8 proved that the incorporation of CDs and AuNCs would not affect the morphology and size of ZIF-8. We consider that the formation of CDs/AuNCs@ZIF-8 nanocomposites may result from the following three coordination interactions: (1) the coordinative interaction between Zn²⁺ and the imidazole molecules in ZnN₄ tetrahedron of ZIF-8 [41], (2) the coordinative interaction between Zn²⁺ and -NH on the CDs surface [42],

Scheme 1 Schematic illustration of the strategy for the detection of Cu²⁺

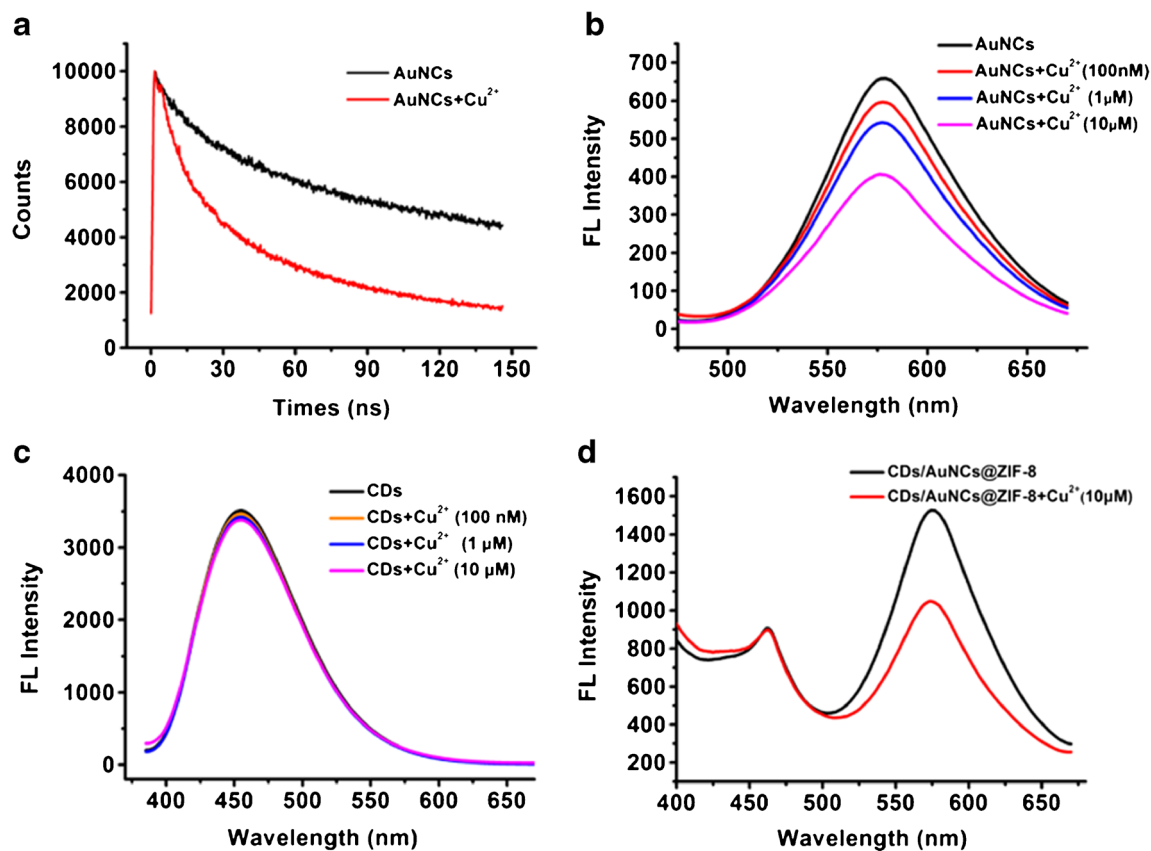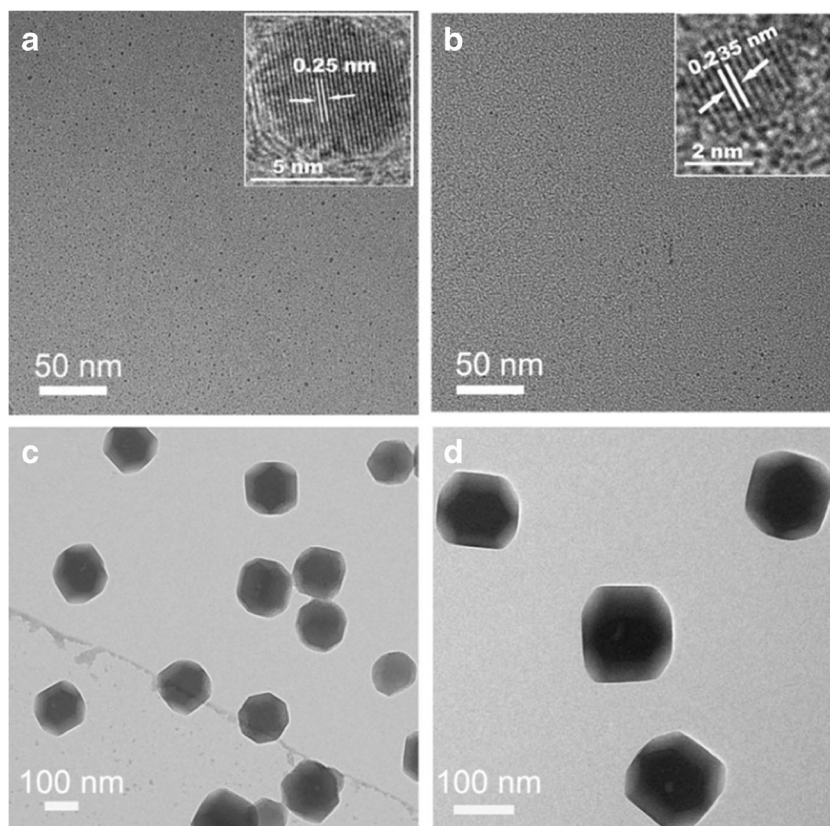

CDs   AuNCs   Quenched AuNCs   CDs/AuNCs@ZIF-8
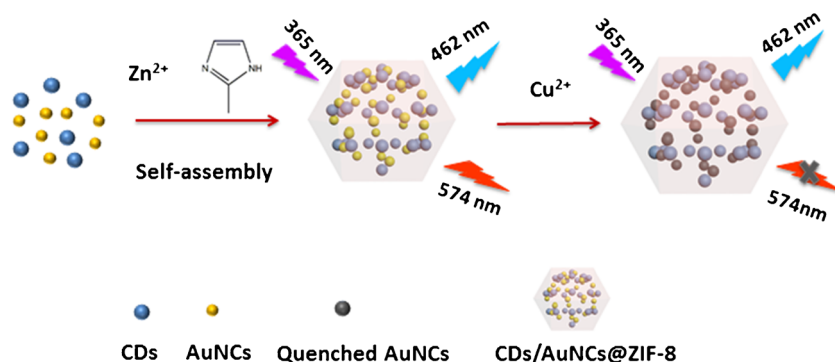
Fig. 1 **a** The fluorescence lifetime decay of AuNCs in the absence or presence of Cu^{2+}. Fluorescence emission spectra of **b** AuNCs, **c** CDs, and **d** CDs/AuNCs@ZIF-8 in the absence and presence of Cu^{2+}

Fig. 2 TEM images of **a** CDs, **b** Au NCs, **c** ZIF-8, and **d** CDs/AuNCs@ZIF-8

(3) the coordinative interaction between Zn^{2+} and -COOH in GSH of AuNCs [31]. These interactions led to the formation of CDs/AuNCs@ZIF-8.

In order to deeply confirm the forming process of CDs/AuNCs@ZIF-8 nano composites, the FTIR spectra measurement was performed. As shown in Fig. 3, the FTIR spectrum for the CDs was dominated by bands at ~3130, 1580, and 1420 cm^{-1}, which were attributed to amine and hydroxyl groups, C=O and C=C stretching vibrations and C–N bending vibrations, respectively [35]. The FTIR spectrum for the AuNCs showed a distinct absorption peak at ~3400 cm^{-1}, which could be assigned to -OH stretching vibrations. It could be seen that the absorption peaks at 1580 and 1420 cm^{-1} of CDs and 3400 cm^{-1} of AuNCs were also observed in the spectrum of the CDs/AuNCs@ZIF-8 nanocomposites while that was not found in the spectrum of pure ZIF-8. On the basis of these results, we concluded that the CDs/AuNCs@ZIF-8 composites were prepared successfully.

The optical properties of CDs/AuNCs@ZIF-8 were investigated by UV-vis absorption spectra and fluorescence spectra. Figure 4 showed UV-vis absorption spectra of the CDs (red), AuNCs (black), pure ZIF-8 (pink), and CDs/AuNCs@ZIF-8 nanocomposites (blue). In the range of 300–600 nm, the CDs exhibited an absorption peak at 345 nm and the AuNCs displayed an absorption peak at 365 nm, which matched well with results in literatures [35, 36]. The pure ZIF-8 had a very weak absorption band while the CDs/AuNCs@ZIF-8 nanocomposites had a strong absorption band in UV-vis range. These results indicated that CDs and AuNCs were embedded deeply into the dense ZIF-8 matrix. In addition, the fluorescence spectrum of CDs/AuNCs@ZIF-8 nanocomposites with different volume AuNCs and CDs were recorded by fluorescence spectrometer. The obtained results (see Fig. S2 in the ESM) proved the fluorescence intensity of CDs/AuNCs@ZIF-8 could be regulated by varying the volume of AuNCs and CDs solution.
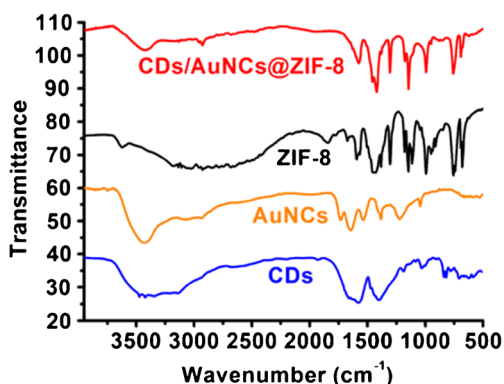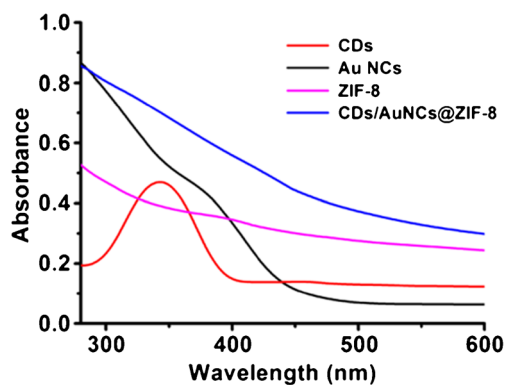

Fig. 4 UV spectra of CDs, AuNCs, ZIF-8 and CDs/AuNCs@ZIF-8

Optimization of experimental conditions

To get the excellent detection performance, the experimental conditions such as pH, reaction temperature, and the type of buffer solution were optimized. Considering that the pH may affect the structure of ZIF-8, it is optimized firstly. It can be seen from Fig. S3a (see the ESM) that the pH had remarkable influence on the change of fluorescence intensity ratio ($\triangle F_{574}/F_{462}$). ($\triangle F_{574}/F_{462}$ means the changed value of fluorescence intensity ratio of the CDs/AuNCs@ZIF-8 in the absence and presence of Cu^{2+}.) At pH 7.4, the $\triangle F_{574}/F_{462}$ reached a maximum; therefore, pH 7.4 was chosen as the optimal pH for Cu^{2+} detection. In addition, the influence of the reaction temperature on the $\triangle F_{574}/F_{462}$ was also investigated (see Fig. S3b in the ESM). The results showed that the $\triangle F_{574}/F_{462}$ reached the maximum at 37 °C. Thus, we chose 37 °C as the optimal reaction temperature for Cu^{2+} detection in the further experiments. Lastly, taking into account that different buffer solutions contain different components, some of components may interact with Cu^{2+} to affect the experimental results. Therefore, the types of buffer solutions were optimized. The results indicated that the $\triangle F_{574}/F_{462}$ reached a maximum in PBS buffer (see Fig. S3c in the ESM); therefore, next experiments were completed in PBS buffer.

Performance for Cu^{2+} detection

The CDs/AuNCs@ZIF-8 nanoprobe was applied to detect Cu^{2+}. As shown in Fig. 5a, with the increase of Cu^{2+} concentrations, the fluorescence peak of CDs/AuNCs@ZIF-8 located at 462 nm remained almost unchanged, while the fluorescence peak at 574 nm was quenched obviously. A good fitted regression line between the fluorescence intensity ratio F_{574}/F_{462} and Cu^{2+} concentrations was obtained in the range of 10^{-3} to 10^{3} μM (Fig. 5b), with a linear regression equation as $Y = 0.9732 – 0.1595 \log C$ (C was the concentration of Cu^{2+} (μM), $R^2 = 0.9928$). The detection limit of Cu^{2+} is estimated to be 0.3324 nM according to the 3σ rule. These results demonstrated that the current strategy was more sensitive compared to
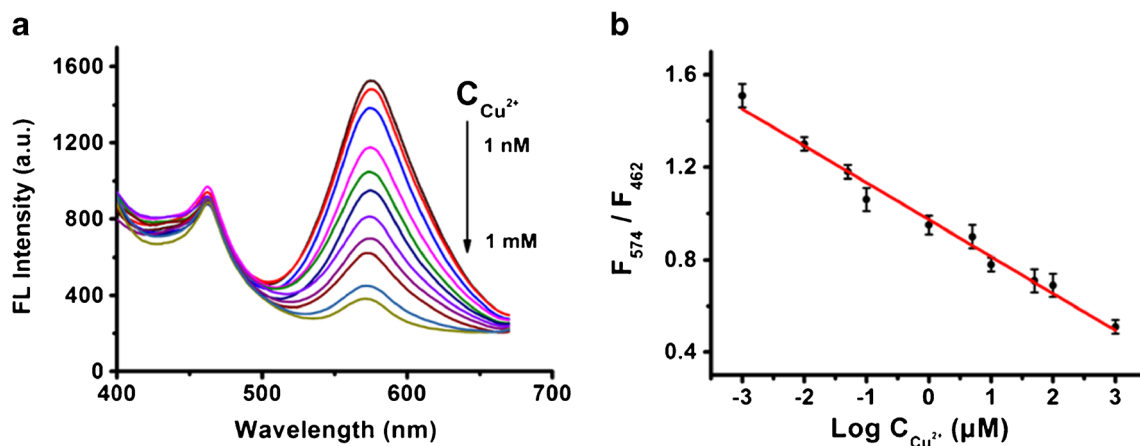

Fig. 3 FTIR spectra of CDs, AuNCs, ZIF-8 and CDs/AuNCs@ZIF-8

Fig. 5 **a** Fluorescence emission spectra of CDs/AuNCs@ZIF-8 in the presence of various Cu^{2+} concentrations (1 nM–1 mM). **b** Relationship between the fluorescence intensity ratio F_{574}/F_{462} and Cu^{2+} concentrations. (F_{574} and F_{462} are the fluorescence intensities of CDs/AuNCs@ZIF-8 at 574 nm and 462 nm, respectively)

most of the previous reported methods for Cu^{2+} determination (see Table S2 in the ESM).

Selectivity and interference studies

In addition to the sensitivity, selectivity is another significant factor to evaluate the potential applications of a newly designed detection system in a real sample. To investigate the selectivity of the CDs/AuNCs@ZIF-8 nanoprobe for Cu^{2+}, some potential interferents, such as inorganic ions (Na^+, Fe^{3+}, Zn^{2+}, Mg^{2+}, Fe^{2+}, Pb^{2+}, Al^{3+}, Ca^{2+}), amino acids (Cys, Gly, Phe, Tyr, Glu, and Asp), and other biological molecules (GSH), were tested under the same conditions. As shown in

Fig. 6a, the fluorescence response (F_{574}/F_{462}) of this nanoprobe was immensely decreased by Cu^{2+}. However, no obvious interferences were observed for other substance including inorganic ion, glutathione, and some amino acids. The result indicated that this designed fluorescence detection system possessed a high selectivity toward Cu^{2+}. Besides, interference experiments were also performed and the results were showed in Fig. 6b. Interfering substances had no significant impact on ratio fluorescence intensity F_{574}/F_{462} of CDs/AuNCs@ZIF-8 containing Cu^{2+}. All the above results manifested that this method had high selectivity and anti-interference ability, which may be directly applied to detect Cu^{2+} in real samples.
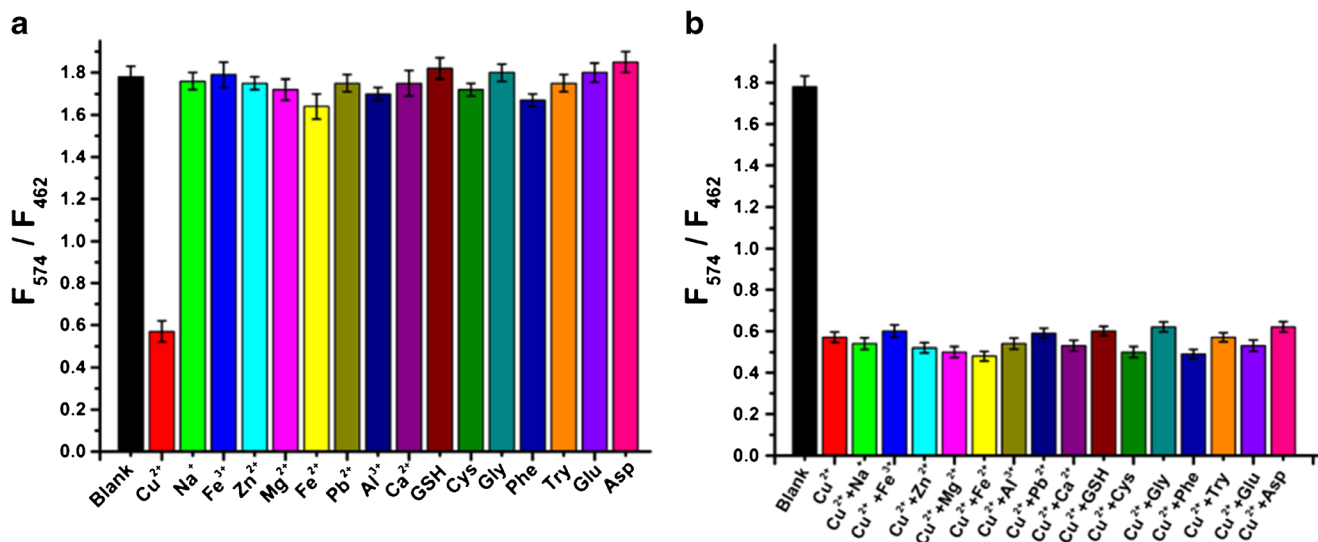

Fig. 6 **a** Fluorescence intensity ratio F_{574}/F_{462} of CDs/AuNCs@ZIF-8 for Cu^{2+} over other potential interferences. **b** Fluorescence intensity ratio F_{574}/F_{462} of CDs/AuNCs@ZIF-8 for Cu^{2+} with other potential interferences. (The concentration of all metal ions is 10 μM; the concentration of amino acids and GSH is 1 μM). The error bars were derived from the standard deviation of three measurements. Error bar = SD ($n = 3$)

Embedding carbon dots and gold nanoclusters in metal-organic frameworks for ratiometric fluorescence...

1323

Table 1 Recoveries results of the determination of Cu^{2+} in serum samples

Sample	Found (μM)	Added (μM)	Total (μM)	Recovery (%)	RSD (n = 3, %)
1	0.13	20.00	21.02	104.5	4.3
		50.00	49.50	98.7	3.3
		100.00	101.20	101.1	3.5
2	0.18	20.00	20.89	103.6	3.8
		50.00	51.30	102.2	2.7
		100.00	99.20	99.0	2.0
3	0.16	20.00	19.35	95.6	4.5
		50.00	51.04	101.8	3.3
		100.00	101.01	100.9	2.1

Determination of Cu^{2+} in real samples

To explore the practical application of the developed method, we applied this nanoprobe to analyze Cu^{2+} in serum samples using the standard addition method. As listed in Table 1, the original Cu^{2+} concentrations in the three human serum samples (1%) were 0.13, 0.18, and 0.16 μM, respectively, which were in the normal range of 11.00–24.39 μM without dilution. Next, Cu^{2+} with different concentrations (20 μM, 50 μM, 100 μM) was added into each serum samples, the recovery of Cu^{2+} was ranged from 95.49 to 104.4%, and the RSD was ranged from 2.1 to 4.5%. That indicated the precision and accuracy of the method for Cu^{2+} determination in real samples.

Conclusion

In summary, a metal-organic framework–based dual-emission fluorescent nanoprobe had been prepared for the detection of Cu^{2+}. The nanohybrids CDs/AuNCs@ZIF-8 were used as a novel sensing nanoprobe for label-free and sensitive detection of Cu^{2+} with the detection limit of 0.3324 nM. Moreover, the practical application of the nanoprobe was validated through the detection of Cu^{2+} in serum samples with satisfactory results. The present study offered a ratiometric fluorescent nanoprobe for detecting Cu^{2+} and opened a new direction for the development of ratiometric fluorescent methods based on nanomaterials embedded into ZIF-8 nanostructures for practical applications.

Compliance with ethical standards

Ethical committee approval The human serum sample experiments were performed in strict accordance with the guidelines from the Ethical Committee, Qufu Normal University. All serum samples were obtained from healthy college student volunteers with their informed consent. All studies were approved by the Ethical Committee of Qufu Normal University.

Conflict of interest The authors declare that they have no conflict of interest.

References

1. Cotruvo JJ, Aron AT, Ramos-Torres KM, Chang CJ. Synthetic fluorescent probes for studying copper in biological systems. Chem Soc Rev. 2015;44:4400–14.

2. Andrási E, Farkas É, Scheibler H, Réffy A, Bezúr L. Al, Zn, Cu, Mn and Fe levels in brain in Alzheimer's disease. Arch Gerontol Geriatr. 1995;21:89–97.

3. Yatsunyk LA, Rosenzweig AC. Cu (I) binding and transfer by the N terminus of the Wilson disease protein. J Biol Chem. 2007;282:8622–31.

4. Viles JH. Metal ions and amyloid fiber formation in neurodegenerative diseases. Copper, zinc and iron in Alzheimer's, Parkinson's and prion diseases. Coord Chem Rev. 2012;256:2271–84.

5. Shen QP, Li WH, Tang SY, Hu YF, Nie Z, Huang Y, et al. A simple "clickable" biosensor for colorimetric detection of copper (II) ions based on unmodified gold nanoparticles. Biosens Bioelectron. 2013;41:663–8.

6. Park Y, Lee CY, Park KS, Park HG. Enzyme-free colorimetric detection of Cu^{2+} by utilizing target-triggered DNAzymes and toehold-mediated DNA strand displacement events. Chem Eur J. 2017;23:17379–83.

7. Zhao L, Li HY, Xu Y, Liu HC, Zhou TY, Huang N, et al. Selective detection of copper ion in complex real samples based on nitrogen-doped carbon quantum dots. Anal Bioanal Chem. 2018;410:4301–9.

8. Wang CX, Yang F, Tang YS, Yang W, Zhong HL, Yu CC, et al. Graphene quantum dots nanosensor derived from 3D nanomesh graphene frameworks and its application for fluorescent sensing of Cu^{2+} in rat brain. Sensors Actuators B Chem. 2018;258:672–81.

9. Zhou M, Han L, Deng DM, Zhang Z, He HB, Zhang L, et al. 4-mercaptobenzoic acid modified silver nanoparticles-enhanced electrochemical sensor for highly sensitive detection of Cu^{2+}. Sensors Actuators B Chem. 2019;291:164–9.

10. Cheng CM, Huang Y, Tian XQ, Zheng BZ, Li Y, Yuan HY, et al. Electrogenerated chemiluminescence behavior of graphite-like carbon nitride and its application in selective sensing Cu^{2+}. Anal Chem. 2012;84:4754–9.

11. Liu Y, Wu Y, Guo X, Wen Y, Yang H. Rapid and selective detection of trace Cu^{2+} by accumulation-reaction-based Raman spectroscopy. Sensors Actuators B Chem. 2019;283:278–83.

12. Ding H, Liang CS, Sun KB, Wang H, Hiltunen JK, Chen ZJ, et al. Dithiothreitol-capped fluorescent gold nanoclusters: an efficient probe for detection of copper (II) ions in aqueous solution. Biosens Bioelectron. 2014;59:216–20.

13. Wang J, Li RS, Zhang HZ, Wang N, Zhang Z, Huang CZ. Highly fluorescent carbon dots as selective and visual probes for sensing

copyright ions in living cells via an electron transfer process. Biosens Bioelectron. 2017;97:157–63.

14. Zhang XL, Jing X, Liu T, Han G, Li HQ, Duan CY. Dual-functional gadolinium-based copper (II) probe for selective magnetic resonance imaging and fluorescence sensing. Inorg Chem. 2012;51: 2325–31.

15. Wu XM, Wang H, Yang SX, Tian HY, Liu YG, Sun BG. A novel coumarin-based fluorescent probe for sensitive detection of copper (II) in wine. Food Chem. 2019;284:23–7.

16. Doussineau T, Schulz A, Lapresta-Fernandez A, Moro A, Körsten S, Trupp S, et al. On the design of fluorescent ratiometric nanosensors. Chem Eur J. 2010;16:10290–9.

17. Lee MH, Kim JS, Sessler JL. Small molecule-based ratiometric fluorescence probes for cations, anions, and biomolecules. Chem Soc Rev. 2015;44:4185–91.

18. Xiao HB, Li P, Zhang W, Tang B. An ultrasensitive near-infrared ratiometric fluorescent probe for imaging mitochondrial polarity in live cells and in vivo. Chem Sci. 2016;7:1588–93.

19. Yuan L, Lin WY, Cao ZM, Wang JL, Chen B. Development of FRET-based dual-excitation ratiometric fluorescent pH probes and their photocaged derivatives. Chem Eur J. 2012;18:1247–55.

20. Niu WJ, Shan D, Zhu RH, Deng SY, Cosnier S, Zhang XJ. Dumbbell-shaped carbon quantum dots/AuNCs nanohybrid as an efficient ratiometric fluorescent probe for sensing cadmium (II) ions and l-ascorbic acid. Carbon. 2016;96:1034–42.

21. Rao HB, Liu W, Lu ZW, Wang YY, Ge HW, Zou P, et al. Silica-coated carbon dots conjugated to CdTe quantum dots: a ratiometric fluorescent probe for copper (II). Microchim Acta. 2016;183:581–8.

22. Yang WQ, Ni JC, Luo F, Weng W, Wei QH, Lin ZY, et al. Cationic carbon dots for modification-free detection of hyaluronidase via an electrostatic-controlled ratiometric fluorescence assay. Anal Chem. 2017;89:8384–90.

23. Su DD, Wang MK, Liu Q, Chen JY, Su XG. Dual-emission ratio fluorescence detection of bleomycin based on nitrogen doped graphene quantum dots@gold nanoclusters assembly. Sensors Actuators B Chem. 2019;290:163–9.

24. Zhang LB, Wang EK. Metal nanoclusters: new fluorescent probes for sensors and bioimaging. Nano Today. 2014;9:132–57.

25. Lu WJ, Gao YF, Jiao Y, Shuang SM, Li CZ, Dong C. Carbon nanodots as a fluorescent and colorimetric dual-readout probe for the detection of arginine and Cu^{2+} and its logic gate operation. Nanoscale. 2017;9:11545–52.

26. Aguilera-Sigalat J, Bradshaw D. Synthesis and applications of metal-organic framework-quantum dot (QD@MOF) composites. Coord Chem Rev. 2016;307:267–91.

27. Gao Q, Xu SY, Guo C, Chen YG, Wang LY. Embedding nanocluster in MOF via crystalline ion-triggered growth strategy for improved emission and selective sensing. ACS Appl Mater Interfaces. 2018;10:16059–65.

28. Sun HZ, Cong S, Zheng ZH, Wang Z, Chen ZG, Zhao ZG. Metal–organic frameworks as surface enhanced Raman scattering substrates with high tailorability. J Am Chem Soc. 2019;141:870–8.

29. Chang JF, Wang X, Wang J, Li HY, Li F. Nucleic acid functionalized metal-organic frameworks-based homogeneous electrochemical biosensor for simultaneous detection of multiple tumor biomarkers. Anal Chem. 2019;91:3604–10.

30. Zheng G, de Marchi S, López-Puente V, Sentosun K, Polavarapu L, Pérez-Juste I, et al. Encapsulation of single plasmonic nanoparticles within ZIF-8 and SERS analysis of the MOF flexibility. Small. 2016;12:3935–43.

31. Luo YC, Fan SY, Yu WQ, Wu ZL, Cullen DA, Liang CL, et al. Fabrication of Au_{25} $(SG)_{18}$-ZIF-8 nanocomposites: a facile strategy to position Au_{25} $(SG)_{18}$ nanoclusters inside and outside ZIF-8. Adv Mater. 2018;30:1704576–84.

32. Ma YJ, Xu GH, Wei FD, Cen Y, Ma YS, Song YY, et al. A dual-emissive fluorescent sensor fabricated by encapsulating quantum dots and carbon dots into metal–organic frameworks for the ratiometric detection of Cu^{2+} in tap water. J Mater Chem C. 2017;5:8566–71.

33. Wang J, Chen HY, Ru F, Zhang Z, Mao X, Shan DL, et al. Encapsulation of dual-emitting fluorescent magnetic nanoprobe in metal-organic frameworks for ultrasensitive ratiometric detection of Cu^{2+}. Chem Eur J. 2018;24:3499–505.

34. Lin XM, Gao GM, Zheng LY, Chi YW, Chen GN. Encapsulation of strongly fluorescent carbon quantum dots in metal–organic frameworks for enhancing chemical sensing. Anal Chem. 2013;86:1223–8.

35. Kong WH, Wu D, Li GL, Chen XF, Gong PW, Sun ZW, et al. A facile carbon dots based fluorescent probe for ultrasensitive detection of ascorbic acid in biological fluids via non-oxidation reduction strategy. Talanta. 2017;165:677–84.

36. Luo ZT, Yuan X, Yu Y, Zhang QB, Leong DT, Lee JY, et al. From aggregation-induced emission of Au (I)-thiolate complexes to ultrabright Au (0)@ Au (I)-thiolate core-shell nanoclusters. J Am Chem Soc. 2012;134:16662–70.

37. Pan YC, Liu YY, Zeng GF, Zhao L, Lai ZP. Rapid synthesis of zeolitic imidazolate framework-8 (ZIF-8) nanocrystals in an aqueous system. Chem Commun. 2011;47:2071–3.

38. Yuan YH, Liu ZX, Li RS, Zou HY, Lin M, Liu H, et al. Synthesis of nitrogen-doping carbon dots with different photoluminescence properties by controlling the surface states. Nanoscale. 2016;8: 6770–6.

39. Qian H, Zhu M, Wu Z, Jin R. Quantum sized gold nanoclusters with atomic precision. Acc Chem Res. 2012;45:1470–9.

40. Ding SN, Li CM, Bao N. Off-on phosphorescence assay of heparin via gold nanoclusters modulated with protamine. Biosens Bioelectron. 2015;64:333–7.

41. Li Z, Zeng HC. Surface and bulk integrations of single-layered Au or Ag nanoparticles onto designated crystal planes {110} or {100} of ZIF-8. Chem Mater. 2013;25:1761–8.

42. He L, Wang TT, An JP, Li XM, Zhang LY, Li L, et al. Carbon nanodots@ zeolitic imidazolate framework-8 nanoparticles for simultaneous pH-responsive drug delivery and fluorescence imaging. CrystEngComm. 2014;16:3259–63.